Journal of Nuclear Medicine, published on June 28, 2019 as doi:10.2967/jnumed.119.227801

Image quality and semi-quantitative measurements of the Siemens Biograph Vision PET/CT: Initial experiences and comparison with Siemens Biograph mCT PET/CT

Joyce van Sluis[1*], Ronald Boellaard[1], Ananthi Somasundaram[1], Paul H. van Snick[1], Ronald J.H. Borra[1], Rudi A.J.O. Dierckx[1], Gilles N. Stormezand[1], Andor W.J.M. Glaudemans[1], and Walter Noordzij[1]

*Correspondence: j.van.sluis@umcg.nl

ORCID ID: https://orcid.org/0000-0003-1908-4518

[1]Department of Nuclear Medicine and Molecular Imaging, University of Groningen, University Medical Center Groningen, Groningen, The Netherlands

Running title: First experiences with the Vision PET/CT

Address for correspondence

Joyce van Sluis,

Department of Nuclear Medicine and Molecular Imaging

University Medical Center Groningen

Hanzeplein 1, 9713GZ, Groningen

The Netherlands

Word count: 5449

ABSTRACT

In May 2018 the new Biograph Vision PET/CT (Siemens Healthineers, Knoxville, USA) was introduced at the University Medical Center Groningen. This study evaluated the initial experiences with this new PET/CT system in terms of perceived image quality and semi-quantitative analysis in comparison to the Biograph mCT (Siemens Healthineers, Knoxville, USA) as a reference.

Methods: A total of 20 oncological patients were enrolled and received a single ^{18}F-FDG injected dose of 3 MBq/kg followed by a dual-imaging PET protocol. Ten patients were scanned on the Biograph mCT first, while the other ten patients were scanned on the Biograph Vision first. The locally preferred clinical reconstructions were blindly reviewed by three nuclear medicine physicians and scored 1-5 on tumor lesion delineation, overall image quality, and image noise. In addition, these clinical reconstructions were used for semi-quantitative analysis; measurement of standardized uptake values (SUVs) in tumor lesions. Reconstructions conform the European Association of Nuclear Medicine Research Ltd (EARL) specifications were also used for measurements of SUVs in tumor lesions and healthy tissues for comparison between systems.

Results: 20 oncological patients (14 men, 6 women; age 36-84, mean ± SD 61 ± 16 years) received a single ^{18}F-FDG injected dose (range 145-405 MBq, mean ± SD 268 ± 59.3). Images acquired on the Biograph Vision were scored significantly higher on tumor lesion delineation, overall image quality, and image noise in comparison to images acquired on the Biograph mCT ($P < 0.001$). The overall inter-reader agreement showed a Fleiss kappa of 0.61 (95% CI 0.53 – 0.70). Furthermore, the measured SUVs in tumor lesions and healthy tissues showed a good agreement (within 95%) between PET/CT systems, in particular when using EARL compliant reconstructions on both systems.

Conclusions: In this initial study it was found that the Biograph Vision PET/CT showed improved image quality compared with the Biograph mCT in terms of lesion demarcation, overall image quality, and

visually assessed signal-to-noise ratio. The two systems are comparable in semi-quantitatively assessed image biomarkers in both healthy tissues and tumor lesions. Improved quantitative performance may, however, be feasible using the clinically optimized reconstruction settings.

Keywords: PET/CT, silicon photomultipliers, standardized uptake value, image quality

INTRODUCTION

Positron Emission Tomography (PET) integrated with Computed Tomography (CT) is a standard of care used in oncology *(1–3)* and many other indications, such as infectious diseases, cardiology and neurology. In oncology, PET/CT is a commonly used and rapidly evolving technique for, among others, differentiation between benign and malignant tumors, cancer staging, primary tumor definition, therapy prediction and guidance, and for radiation therapy planning *(1,3)*.

Improvements in PET instrumentation over the years include for example the use of fast lutetium oxyorthosilicate (LSO) crystals permitting the use of shorter coincidence timing windows *(4,5)*, new reconstruction methods with Time-of-Flight (TOF) application *(5–9)* for improved image signal-to-noise ratio, and expansion of the axial field-of-view (FOV) for increased volume sensitivity and axial coverage *(9)*. Recently, silicon photomultiplier (SiPM) based detectors emerged offering several advantages over photomultiplier tubes (PMTs) such as compact size, higher intrinsic time resolution, and high photon-detection efficiency making them favorable for coupling with TOF reconstruction *(10,11)*.

The most commonly used PET radiotracer at present is 2-deoxy-2-[fluorine-18]fluoro-D-glucose (^{18}F-FDG), a glucose analog, which accumulation in tissue is proportional to glucose utilization *(1)*. Based on increased glucose uptake and glycolysis of specific tumors, ^{18}F-FDG PET/CT has been proven to be essential in detection, staging, therapy planning and evaluating treatment responses in oncology *(12–16)*.

In May 2018, the first SiPM-based Biograph Vision PET/CT system (Siemens Molecular Imaging, Knoxville, USA) was installed at the department of Nuclear Medicine and Molecular Imaging at the University Medical Center Groningen. The 3.2 mm crystal size allows for a high system spatial resolution, and full coverage of the small crystals by the SiPM detector elements optimizes light collection enabling improved timing resolution and signal-to-noise ratio *(17)*.

The main purpose of this study was to evaluate initial clinical experiences and to explore whether the newly developed system yields improved image quality and diagnostic performance (i.e., lesion demarcation, overall image quality, and visually assessed signal-to-noise ratio) in comparison with its predecessor, the Biograph mCT. Therefore, a comparison between whole-body ^{18}F-FDG clinical images obtained on the Biograph Vision and the Biograph mCT (Siemens Healthineers, Knoxville, USA), that are both systems of the same vendor, has been explored both visually and semi-quantitatively.

MATERIALS AND METHODS

Patient Population

Between June and August 2018, 20 patients who were referred to the department of Nuclear Medicine and Molecular Imaging for an oncological clinical PET/CT were enrolled in this prospective study. Patients with a glucose level of $\geq$ 198 mg/dl prior to ^{18}F-FDG injection were excluded as well as pregnant women, and patients unable to lie still for the duration of the exam.

The local medical ethics review board of the University Medical Center Groningen waived the need for formal ethical review (waiver number: METc2017/489) upon proposal and review of the study protocol. In addition, patients were informed about the study aims, procedures, and the acquisition of an additional low dose CT ($\sim$1 mSv) and written informed consent was obtained from each patient before inclusion.

Imaging Protocol

All patients received a single weight-based dose injection of ^{18}F-FDG (3 MBq/kg according to European Association of Nuclear Medicine guidelines) *(18)*, followed by a dual-imaging PET protocol including a PET/CT scan on the Biograph Vision and a PET/CT scan on the Biograph mCT. Ten patients first underwent acquisition on the Biograph mCT 60 min post injection, followed immediately by image acquisition using the Biograph Vision, approximately 90 min post injection. In the other ten patients the scanner order of image acquisition was switched to control for tumor metabolic activity increase over time, possibly influencing image quality. Since the PET/CT systems at the department of Nuclear Medicine and Molecular Imaging at the University Medical Center Groningen are accredited for ^{18}F-FDG PET/CT imaging by the European Association of Nuclear Medicine Research Ltd (EARL), the EARL imaging protocol is followed strictly. The EARL imaging protocol recommends the scan start to be at 60 min post-injection *(1,19)*. Second scans were done immediately following the first, therefore, ^{18}F-FDG uptake time and time delay between scans were comparable for all 20 cases.

Participants were instructed to fast and avoid strenuous exercise for at least 4-6 hours prior to intravenous ^{18}F-FDG injection. At the time of ^{18}F-FDG dose administration, blood glucose levels were $\leq$ 198 mg/dl. A standard low dose CT was obtained from the top of the head to the mid-thighs and used for attenuation correction. The parameters of the standard low dose CT scan obtained on the Biograph Vision used for the attenuation correction were: an X-ray tube current of 43 mAs, a tube voltage of 100 keV, and a spiral pitch factor of 1. The parameters of the low dose CT scan obtained on the 40-slice and 64-slice Biograph mCT were, respectively: an X-ray tube current of 103 mAs and 99 mAs, a tube voltage of 140 keV and 140 keV, and a spiral pitch factor of 1 and 1.5. Following the low dose CT, an emission PET scan was acquired in 3 minutes per bed position in list mode. All scans were acquired during normal breathing without respiratory motion gating or correction.

Images acquired on the Biograph Vision were reconstructed using the vendor recommended, clinically most relevant, reconstruction protocol, i.e., an ordinary Poisson ordered-subset expectation maximization (OP-OSEM) 3D-iterative algorithm *(20)* with 4 iterations and 5 subsets, with application of TOF and resolution modelling, without filtering. Resulting PET images had an image matrix size of 440x440 with a voxel size of 1.6x1.6x1.5 mm. Images acquired on the Biograph mCT were reconstructed using the locally preferred clinical reconstruction protocol: 3D TOF OP-OSEM with 3 iterations, 21 subsets, and resolution modelling. A Gaussian filter of 5 mm was applied to the reconstructed images, and the resulting image size was 400x400 with a voxel size of 2x2x2 mm. In addition, the EARL *(1,19)* reconstructions for both the Biograph Vision and the Biograph mCT were obtained. Images acquired on the Vision were reconstructed to comply to EARL using 3D TOF OP-OSEM, with 4 iterations and 5 subsets, with application of resolution modelling and a Gaussian filter of 7 mm. The resulting image size was 440x440 with a voxel size of 1.6x1.6x1.5 mm. EARL reconstruction for images obtained from the Biograph mCT was done using 3D TOF OP-OSEM with 3 iterations and 21 subsets, resolution modelling and a Gaussian filter of 6.5 mm into an image matrix size of 256x256 with a voxel size of 3.2x3.2x2 mm.

Qualitative Image Analysis

The acquired images were independently reviewed and analyzed using a dedicated *syngo.*via VB30 (Siemens Healthineers) workstation. All PET reconstructions acquired from the recommended clinical reconstruction protocols were blindly evaluated by three experienced nuclear medicine physicians (AG, GS and WN: 15, 5 and 10 years of experience in interpreting PET scans, respectively). The readers were not aware of the clinical indication for the PET/CT.

Readers were allowed to manually adjust the standard window settings. Subsequently, based on 5-point Likert-scales, the following quality criteria were assessed: tumor lesion delineation (ranging from 1 = lesion cannot be confirmed to 5 = excellent lesion margin delineation), overall image quality (ranging from 1 = poor overall image quality to 5 = excellent overall image quality), and image noise (ranging from 1 = enormous image noise to 5 = no perceivable image noise) *(10,21)*. In addition, per clinically recommended reconstruction, the number of suggestive ^{18}F-FDG-avid lesions were counted. In case of large assessment differences between readers, the specific images were discussed in a consensus meeting.

Semi-quantitative Image Analysis

Semi-quantitative analyses were performed using the quAntitative onCology moleCUlar Analysis suiTE (ACCURATE) *(22)*. Using the EARL reconstructed images, 0.5-mL-spherical volumes of interest (VOIs) were placed in healthy tissues (aortic arch, semioval center (white matter), lung, left ventricle of the heart, parotid gland, quadriceps femoris muscle, the spleen) and for reference tissue purposes, a 3-mL-sperical VOI was placed in the liver. From these VOIs maximum, peak, and mean standardized uptake values (SUVmax, SUVpeak, and SUVmean) were obtained. In addition, using the EARL reconstructed images as well as the locally preferred clinical reconstructed images, VOIs were placed in the different lesions per patient (with an overall maximum of five lesions per patient, with a maximum of two in the

same tissue type). From these measurements, the different SUVmax, SUVpeak, and SUVmean were compared between systems.

Statistical Analysis

Statistical analysis was performed with SPSS Statistics, version 25.0 (IBM Corp., Armonk, NY). Scoring of the images acquired on the two PET/CT systems were compared pairwise using a two-tailed paired samples t-test. For inter-reader agreement regarding tumor lesion delineation, overall image quality, and image noise, the original 5-point scores were reassigned to 3-point scores (1 + 2 became 1, 3 became 2, and 4 + 5 became 3). Inter-reader agreement was subsequently evaluated using kappa statistic. Bland-Altman plot analysis was performed to assess the agreement regarding SUVmax, SUVpeak, and SUVmean obtained in healthy tissues and in lesions between the two systems. Subsequently, equivalence tests were done on each of the healthy tissues and on the tumor lesions to quantify the agreement regarding the SUVs between the different systems. Furthermore, using partial correlation, the relation between different SUVs and time delay between scans was evaluated.

RESULTS

A total of 20 oncological patients (14 men, 6 women; age 36-84, mean ± SD 61 ± 16 years) were enrolled in the study. To simulate the actual clinical experience, different cancer types were included. Table 1 shows relevant demographic and clinical information. The injected ^{18}F-FDG dose ranged from 145-405 MBq (mean ± SD 268 ± 59.4). All patients had a blood glucose level of $\leq$ 198 mg/dl prior to dose administration. To control for changes in ^{18}F-FDG uptake over time possibly influencing image quality, the first ten patients were scanned on the Biograph mCT first, whereas the other ten patients were scanned on the Biograph Vision first. The time delay between the start of the first and the start of the second scan ranged from 24 – 60 min (mean ± SD 37 ± 7.7).

Qualitative Image Quality

The average scores ± SD of all three readers for the Biograph mCT images versus Biograph Vision images on lesion delineation were 3.3 ± 1.0 versus 4.3 ± 0.80, on overall image quality 3.4 ± 0.90 versus 4.3 ± 0.80, and on image noise 3.4 ± 0.70 versus 3.9 ± 0.70. Images acquired on the Biograph Vision were scored significantly higher on tumor lesion delineation (median 5), overall image quality (median 4), and image noise (median 4) with respect to images acquired on the Biograph mCT scoring median values of 3, 3, and 3, for the different categories, respectively ($P < 0.01$). The overall inter-reader agreement showed a Fleiss kappa of 0.61 (95% CI 0.53 – 0.70). For illustrative purposes, images of patients of standard weight (91 kg and 101) are shown in Figures 1 and 2. Supplemental Figures 1 and 2 show images of a lighter weight (53 kg) and a heavier weight (139 kg) patient, respectively.

In 7 of 20 patients, one or more additional ^{18}F-FDG avid lesions were identified on the Biograph Vision images with respect to the Biograph mCT images. These additional lesions all measured below 0.75 cm in diameter and were found in areas with significant motion, e.g., in the lungs and near the

diaphragm. See Figures 3 and 4 for illustrative examples of the additional lesions found on the Biograph Vison images with respect to the images from the Biograph mCT.

Semi-quantitative Image Quality

The results of the equivalence tests of SUV measurements in healthy tissue matched per patient are presented in Table 2. There was a good agreement in SUVs measured in tumor lesions and healthy tissues between the two PET/CT systems when using EARL compliant reconstructions. For illustrative purposes, Bland-Altman plots to display the agreement of SUVmax measurements in normal tissues acquired on the two systems are shown in supplemental Figure 3. Results of the equivalence tests of SUVmax, SUVpeak, and SUVmean measurements in tumor lesions are presented in Table 3. There was no significant difference in ^{18}F-FDG uptake between SUVmax, SUVpeak, and SUVmean measurements obtained on images acquired from the two systems. The agreement of tumor lesion SUVmax, SUVpeak, and SUVmean measurements between the two systems is shown in the Bland-Altman plots in Figure 5. Scatter plots of lesion SUVs derived from images obtained from the two systems are displayed in supplemental Figure 4. For illustrative purposes, SUVmax, SUVpeak, and SUVmean distributions between EARL compliant and clinically reconstructed images acquired on the two systems are shown in boxplots in Figure 6.

Partial correlation showed no significant correlation between normal tissue SUVmax, SUVpeak, SUVmean, and the time delay between systems. There was no correlation between lesion SUVmax, SUVpeak, SUVmean, and the time delay between systems either.

Furthermore, SUVs of the additional lesions found on the images obtained on the Vision system were compared to SUVs obtained from the mCT derived images. Lesion SUVmax from the images obtained on the Vision ranged from 4.5 – 34.5 (median: 7.5). The lesion SUVmax derived from the mCT

images ranged from 2.1 – 8.7 (median: 2.9). Additional lesion SUVpeak and SUVmean were similar between systems.

DISCUSSION

In this study, initial experiences with the Biograph Vision were evaluated. The first results indicate that this system outperforms its predecessor, the Biograph mCT, in terms of visually assessed image quality; tumor lesion demarcation, overall image quality, and signal-to-noise ratio. Semi-quantitative analyses show both systems are comparable in assessing biomarkers in both healthy tissues and tumor lesions. Furthermore, in 7 of 20 patients, one or more additional ^{18}F-FDG avid lesions were identified on the Biograph Vision in comparison to the Biograph mCT images, which could have important clinical consequences.

Recent technical developments in PET instrumentation have likely contributed to the improved image quality observed in images acquired on the Vision PET/CT system *(23)*. The introduction of SiPM detectors in commercially available PET/CT systems is of clinical importance due to the potential advantages of the new technology. SiPM-based photodetectors are characterized by superior timing resolution, enabling improved TOF estimation *(24)*, and efficient photon detection.

The performance characteristics of the latest developed SiPM-based PET/CT, the Biograph Vision, were evaluated and published recently by our group *(25)*. Spatial resolution, sensitivity, count-rate performance, accuracy of attenuation and scatter correction, TOF performance, and image quality were evaluated according to the National Electrical Manufacturers Association (NEMA) NU-2 2012 and NEMA NU-2 2018 standards showing improved performance with regard to its predecessor, the Biograph mCT *(25)*. Of all the current commercially available PET/CT systems, the Biograph Vision also outperforms other SiPM-based systems for instance, with a timing resolution of 210 ps compared to 310 ps acquired on the Vereos (Philips Healthcare) *(26)* and 375 ps acquired on the Discovery MI (GE Healthcare) *(3)*. The sensitivity of the Biograph Vision system also improved with regard to the other available SiPM-based

systems measuring 16.4 kcps/MBq on the Biograph Vision, with respect to 5.2 kcps/MBq on the Vereos, and 13.7 kcps/MBq on the Discovery MI.

Benefits of a higher sensitivity and improved TOF resolution are: a higher signal-to-noise ratio (especially for heavy patients), improved overall image quality, improved lesion detectability, and more accurate image quantification *(24)*. Three of these categories have been qualitatively assessed in this study to see whether theoretical and expected improvement in image quality also translates to an improved perceived image quality in clinical practice. It was found that the Biograph Vision scored significantly higher than the Biograph mCT on lesion delineation, overall image quality, and image noise.

With regard to the semi-quantitative measurements, a good agreement was seen in SUVs measured in tumor lesions, and healthy tissues between the Biograph Vision and the Biograph mCT when using EARL compliant reconstructions, as well as when using the locally preferred clinical image reconstructions. Because of the balanced order in which the dual scans were performed (ten patients were scanned first on the Biograph mCT and the other ten patients were scanned first on the Biograph Vision) and by following the EARL guidelines for tumor imaging, there was no significant influence of time delay on the measured normal tissue SUVs nor on the measured lesion SUVs. It should be noted that when using the locally preferred clinical reconstruction settings on the Biograph Vision, the higher spatial resolution of the system and the use of smaller voxel sizes result in less partial volume effect; a higher contrast recovery is obtained, resulting in a slight increase in SUVmax data (however not significant, see Figures 5 and 6, and Table 3). Moreover, higher overall SUVs obtained from the locally preferred clinical reconstructed images can be observed with respect to the SUVs derived from the EARL compliant images (Fig. 5). The occasional increase in SUVmax obtained from the locally preferred clinical reconstructed images in Figure 5 can be explained by the characteristics of the lesions. Obtaining an already high SUVmax (> 10) from images acquired on the Biograph mCT will result in an even higher

SUVmax measured on images acquired on the Biograph Vision (due to higher spatial resolution and smaller voxel size).

As mentioned before, the perceived improvement in image quality resulted in the identification of one or more additional ^{18}F-FDG avid lesions in 7 of 20 patients. The additional lesions found in this study were all below 0.75 cm in diameter and were found in areas significant motion, e.g., in the lungs and near the diaphragm. For a single case, finding an additional lesion resulted in upstaging of the disease. In none of the cases therapy was altered since the additional lesions were in close proximity to the primary tumor or numerous other small metastases were already taken into account. However, in this study only a small sample size was included. Nevertheless, these initial findings could suggest that the Biograph Vision would be more beneficial for detecting small lesions which could have clinical impact, e.g., a change in tumor staging or a different choice of therapy.

Since we believe a more valid comparison in image lesion quantification between the two systems can be achieved in more homogeneous groups of oncologic disease, future studies are warranted to explore lesion image quantification more deeply.

CONCLUSION

In this initial study we found that the Biograph Vision provides better perceived image quality than the Biograph mCT; sharper demarcated tumor lesions were seen, a higher valued overall image quality, and a higher visually assessed signal-to-noise ratio. With regard to semi-quantitative image quality, the two systems are comparable in performance on imaging healthy tissues and tumor lesions. Improved quantitative performance may, however, be feasible using the clinically optimized reconstruction settings. Future studies including more homogeneous groups of oncologic disease are warranted to validate our findings and to assess the potential clinical impact of PET imaging using the Biograph Vision.

ACKNOWLEDGEMENTS

The research presented in this study is financially supported by Siemens Molecular Imaging under a collaborative research contract. No other potential conflict of interest relevant to this article was reported.

KEY POINTS

QUESTION: Does the new Siemens Biograph Vision PET/CT system outperform its predecessor, the Siemens Biograph mCT, in terms of perceived image quality and semi-quantitative analysis?

PERTINENT FINDINGS: In a dual imaging study, perceived image quality was compared between images acquired on the Biograph Vision system and the Biograph mCT system in 20 patients referred for an oncological clinical PET/CT. Images obtained from the Biograph Vision resulted in better perceived image quality; sharper demarcated tumor lesions, a higher valued overall image quality, and a visually assessed higher signal-to-noise ratio. With regard to semi-quantitative image quality, the two systems are comparable in performance on imaging healthy tissues and tumor lesions. Improved quantitative performance may, however, be feasible using clinically optimized reconstruction settings.

IMPLICATIONS FOR PATIENT CARE: Using the new Biograph Vision PET/CT could be beneficial for detecting small lesions which could impact tumor staging or influence the choice of therapy.

REFERENCES

1. Boellaard R, Delgado-Bolton R, Oyen WJG, et al. FDG PET/CT: EANM procedure guidelines for tumour imaging: version 2.0. *Eur J Nucl Med Mol Imaging.* 2014;42:328–54.
2. Slomka PJ, Pan T, Germano G. Recent advances and future progress in PET instrumentation. *Semin Nucl Med.* 2016;46:5–19.
3. Hsu DFC, Ilan E, Peterson WT, Uribe J, Lubberink M, Levin CS. Studies of a next-generation silicon-photomultiplier–based time-of-glight PET/CT system. *J Nucl Med*. 2017;58:1511–8.
4. Melcher CL. Scintillation crystals for PET. *J Nucl Med.* 2000;41:1051–5.
5. Rausch I, Cal-González J, Dapra D, et al. Performance evaluation of the Biograph mCT Flow PET/CT system according to the NEMA NU2-2012 standard. *EJNMMI Phys.* 2015;2:1–17.
6. Moses WW. Time of flight in PET revisited. *IEEE Trans Nucl Sci.* 2003;50:1325–30.
7. Surti S, Kuhn A, Werner ME, Perkins AE, Kolthammer J, Karp JS. Performance of Philips Gemini TF PET/CT scanner with special consideration for its time-of-flight imaging capabilities. *J Nucl Med.* 2007;48:471–80.
8. Jakoby BW, Bercier Y, Conti M, Casey ME, Bendriem B, Townsend DW. Physical and clinical performance of the mCT time-of-flight PET/CT scanner. *Phys Med Biol.* 2011;56:2375–89.
9. Jakoby BW, Bercier Y, Watson CC, Bendriem B, Townsend DW. Performance characteristics of a new LSO PET/CT scanner with extended axial field-of-view and PSF reconstruction. *IEEE Trans Nucl Sci.* 2009;56:633–9.
10. Sonni I, Baratto L, Park S, et al. Initial experience with a SiPM-based PET/CT scanner: influence of acquisition time on image quality. *EJNMMI Phys.* 2018;5:9.
11. Ullah MN, Pratiwi E, Cheon J, Choi H, Yeom JY. Instrumentation for time-of-flight positron emission tomography. *Nucl Med Mol Imaging*. 2016;50:112–22.
12. Almuhaideb A, Papathanasiou N, Bomanji J. 18F-FDG PET/CT imaging in oncology. *Ann Saudi Med.* 2011;31:3–13.
13. Avril NE, Weber WA. Monitoring response to treatment in patients utilizing PET. *Radiol Clin North Am.* 2005;43:189–204.
14. Bastiaannet E, Groen B, Jager PL, et al. The value of FDG-PET in the detection, grading and response to therapy of soft tissue and bone sarcomas; a systematic review and meta-analysis. *Cancer Treat Rev.* 2004;30:83–101.
15. Borst GR, Belderbos JSA, Boellaard R, et al. Standardised FDG uptake: A prognostic factor for inoperable non-small cell lung cancer. *Eur J Cancer.* 2005;41:1533–41.
16. de Geus-Oei L-F, van der Heijden HFM, Corstens FHM, Oyen WJG. Predictive and prognostic value of FDG-PET in nonsmall-cell lung cancer. *Cancer.* 2007;110:1654–64.
17. Surti S. Update on time-of-flight PET imaging. *J Nucl Med.* 2015;56:98–105.
18. Boellaard R, Delgado-Bolton R, Oyen WJG, et al. FDG PET/CT: EANM procedure guidelines for tumour imaging: version 1.0. *Eur J Nucl Med Mol Imaging.* 2014;42:328–54.
19. Boellaard R. New developments of EANM oncology PET/CT guidelines and update of the EARL

accreditation standards presentation. Available from the website of EANM Research Ltd.: http://earl.eanm.org/cms/website.php?id=/en/projects/fdg_pet_ct_accreditation/accreditation_specifications.htm. Accessed November 7, 2018.

20. Varrone A, Sjöholm N, Eriksson L, Gulyás B, Halldin C, Farde L. Advancement in PET quantification using 3D-OP-OSEM point spread function reconstruction with the HRRT. *Eur J Nucl Med Mol Imaging.* 2009;36:1639–50.

21. Lenga L, Czwikla R, Wichmann JL, et al. Dual-energy CT in patients with colorectal cancer: Improved assessment of hypoattenuating liver metastases using noise-optimized virtual monoenergetic imaging. *Eur J Radiol.* 2018;106:184–91.

22. Boellaard R. Quantitative oncology molecular analysis suite: ACCURATE. *J Nucl Med.* 2018; 59(supplement 1):1753–1753. Available from: http://jnm.snmjournals.org/cgi/content/short/59/supplement_1/1753

23. Hutton BF, Erlandsson K, Thielemans K. Advances in clinical molecular imaging instrumentation. *Clin Transl Imaging.* 2018;6:31–45.

24. Vandenberghe S, Mikhaylova E, D'Hoe E, Mollet P, Karp JS. Recent developments in time-of-flight PET. *EJNMMI Phys.* 2016;3:3.

25. van Sluis J, de Jong J, Schaar J, et al. Performance characteristics of the digital Biograph Vision PET/CT system. *J Nucl Med.* 2019;(Published ahead of print):jnumed.118.215418.

26. Rausch I, Ruiz A, Valverde-Pascual I, Cal-González J, Beyer T, Carrio I. Performance evaluation of the Philips Vereos PET/CT System according to the NEMA NU2-2012 standard. *J Nucl Med*. 2019;60:561-567.

Table 1 - Demographic and clinical data of all study participants.

Patient #	Age (y)	Sex	Weight (kg)	Disease	Injected ^{18}F-FDG dose (MBq)	Time delay (min)*
1	40	F	73	Ovarian cancer	230	28
2	69	M	90	Colon cancer	270	40
3	79	M	90	Lung cancer	305	38
4	49	M	97.5	Lung cancer	305	40
5	36	M	79.5	Sarcoidosis	220	42
6	84	M	91	Lung cancer	270	42
7	66	F	101	Thyroid cancer	300	29
8	75	M	88.2	Multiple myeloma	280	60
9	66	F	72	Breast cancer	215	32
10	74	M	139	Melanoma	405	33
11	59	M	106	Esophageal cancer	305	30
12	84	M	73	Esophageal cancer	220	33
13	59	M	104	Oropharyngeal cancer	320	37
14	77	M	62	Colon cancer	200	39
15	62	M	77	Esophageal cancer	240	46
16	63	M	105	Lymphoma	300	41
17	52	F	115	Lymphoma	355	36
18	60	F	89	Esophageal cancer	235	35
19	47	F	53	Lung cancer	145	36
20	25	M	79	Testicular cancer	235	24

*Time delay between the first and second scan in minutes. Images were acquired on the Biograph mCT first for the first ten patients. For the other ten patients images were acquired on the Biograph Vision first.

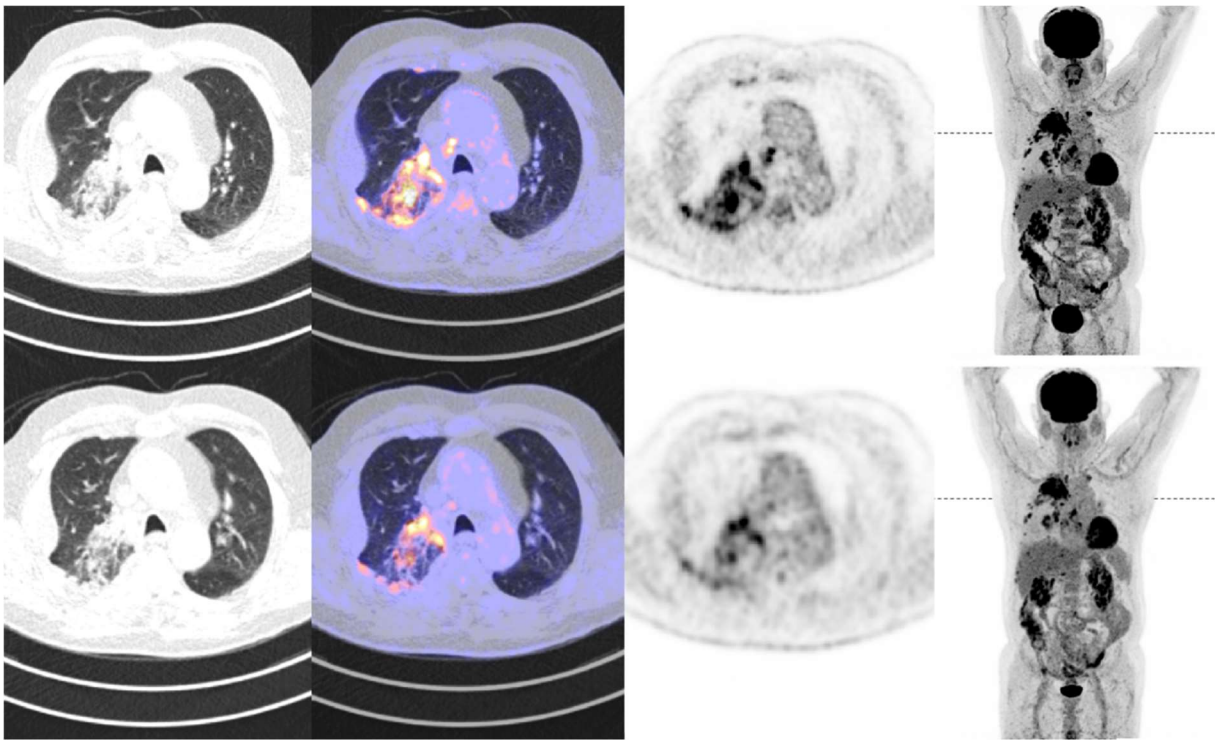

Figure 1 – Illustrative transaxial CT, fusion PET/CT, PET, and maximum intensity projection PET images (from left to right) acquired on the Biograph Vision (upper row) and acquired on the Biograph mCT (lower row) of a 84-year old male patient (weight 91 kg) with metastasized Non-Small Cell Lung Carcinoma. The position of the transaxial slice is indicated on the MIP (dashed line).

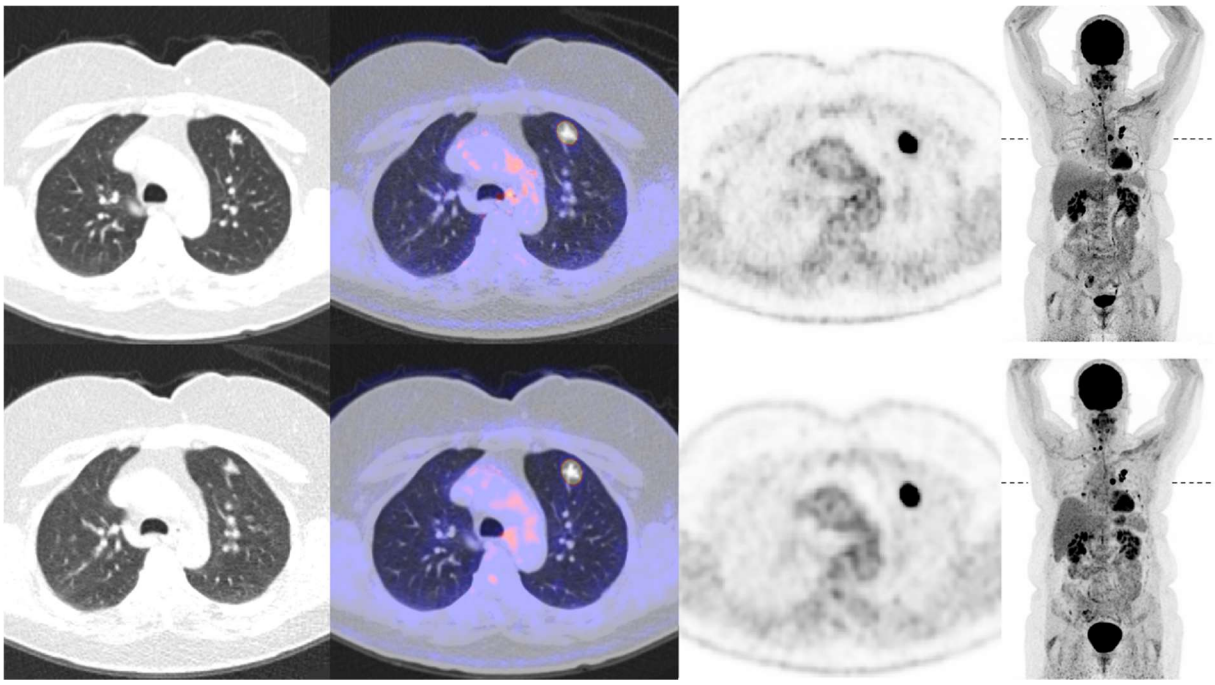

Figure 2 – Illustrative transaxial CT, fusion PET/CT, PET, and maximum intensity projection PET images (from left to right) acquired on the Biograph Vision (upper row) and acquired on the Biograph mCT (lower row) of a 66-year old female patient (weight 101 kg) with metastasized thyroid cancer. The position of the transaxial slice is indicated on the MIP (dashed line).

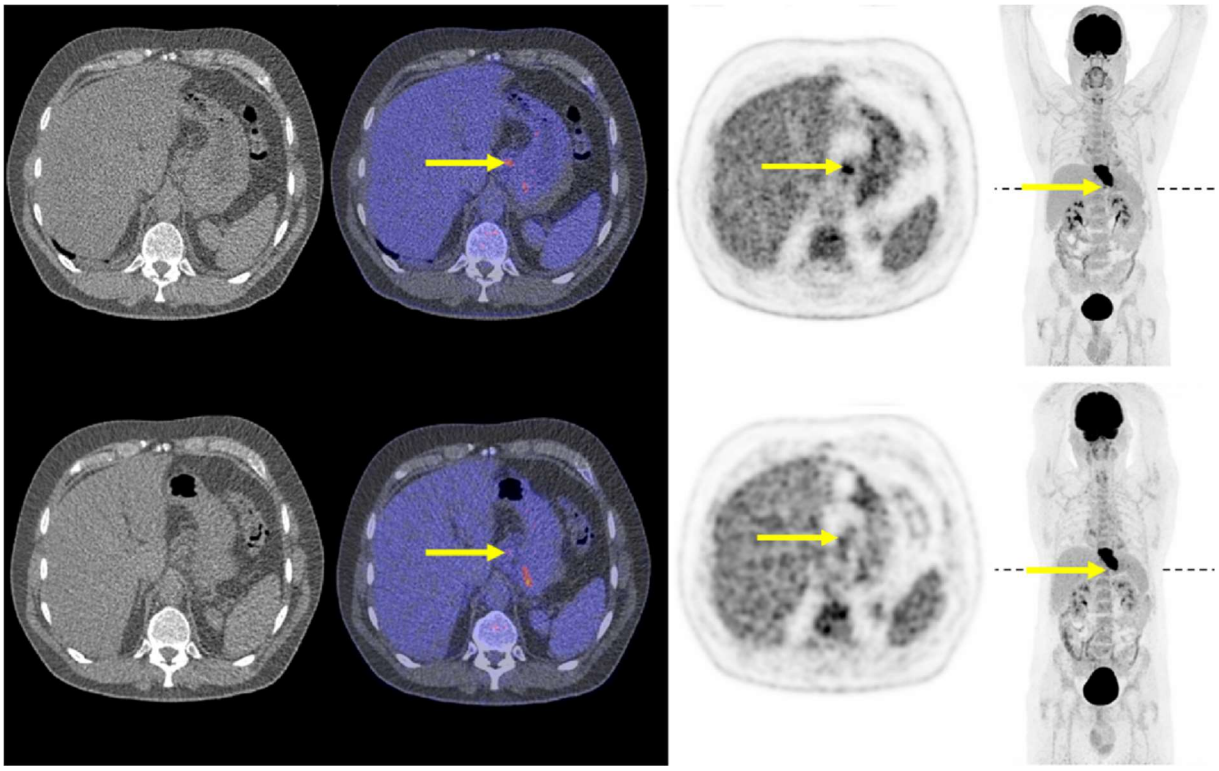

Figure 3 – Illustrative transaxial CT, fusion PET/CT, PET, and maximum intensity projection PET images (from left to right) acquired on the Biograph Vision (upper row) and acquired on the Biograph mCT (lower row) of a 59-year old male patient (weight 106 kg) with metastasized esophageal cancer. The position of the transaxial slice is indicated on the MIP (dashed line). The yellow arrows indicate a small lesion found on the Vision images that did not appear as such on the mCT images.

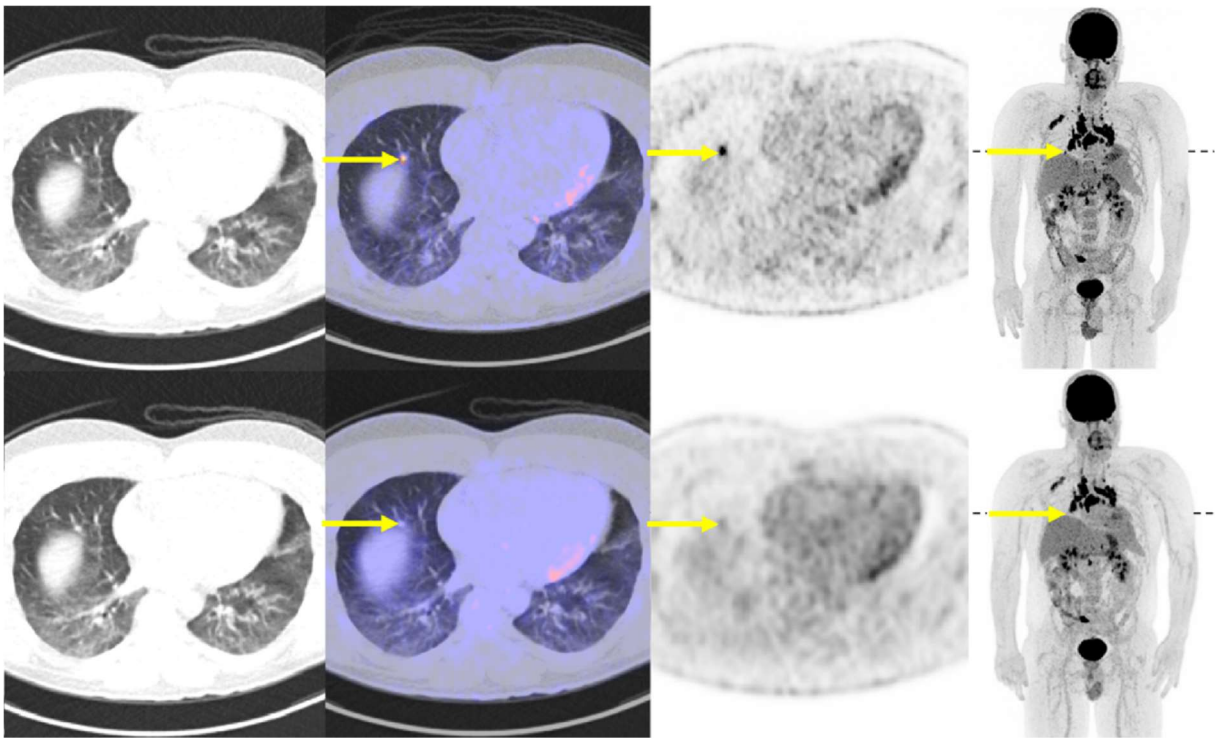

Figure 4 – Illustrative transaxial CT, fusion PET/CT, PET, and maximum intensity projection PET images (from left to right) acquired on the Biograph Vision (upper row) and acquired on the Biograph mCT (lower row) of a 36-year old male patient (weight 69 kg) with sarcoidosis. The position of the transaxial slice is indicated on the MIP (dashed line). The yellow arrows indicate a small lesion found on the Vision images that did not appear as such on the mCT images.

Table 2 - Difference in SUVs in healthy organ tissues.

Organs	Mean difference mCT-Vision SUV±SD		95% CI	P	Equivalence
Aortic arch	SUVmax	-0.01 ± 0.47	-0.23; 0.21	0.921	Equivalent
	SUVpeak	-0.04 ± 0.49	-0.23; 0.23	0.991	Equivalent
	SUVmean	-0.11 ± 0.43	-0.21; 0.20	0.966	Equivalent
Semioval	SUVmax	-0.36 ± 0.83	-0.40; 0.39	0.985	Equivalent
center	SUVpeak	-0.31 ± 0.87	-0.41; 0.40	0.994	Equivalent
	SUVmean	0.01 ± 0.43	-0.20; 0.20	0.997	Equivalent
Liver	SUVmax	0.38 ± 0.28	-0.13; 0.13	0.956	Equivalent
	SUVpeak	-0.11 ± 0.41	-0.19; 0.20	0.968	Equivalent
	SUVmean	0.04 ± 0.28	-0.13; 0.13	0.992	Equivalent
Lung	SUVmax	0.08 ± 0.15	-0.07; 0.07	0.964	Equivalent
	SUVpeak	0.02 ± 0.13	-0.06; 0.06	0.991	Equivalent
	SUVmean	0.04 ± 0.12	-0.06; 0.05	0.867	Equivalent
Left ventricle	SUVmax	0.01 ± 0.65	-0.31; 0.30	0.973	Equivalent
	SUVpeak	-0.16 ± 0.68	-0.32; 0.32	0.987	Equivalent
	SUVmean	0.04 ± 0.53	-0.25; 0.25	0.993	Equivalent
Parotid gland	SUVmax	0.66 ± 0.97	-0.45; 0.45	0.996	Equivalent
	SUVpeak	0.17 ± 0.52	-0.25; 0.24	0.982	Equivalent
	SUVmean	0.57 ± 0.85	-0.40; 0.39	0.979	Equivalent
Quadriceps	SUVmax	0.20 ± 0.30	-0.14; 0.14	0.977	Equivalent
muscle	SUVpeak	0.09 ± 0.23	-0.11; 0.11	0.992	Equivalent
	SUVmean	0.07 ± 0.16	-0.07; 0.07	0.988	Equivalent
Spleen	SUVmax	0.07 ± 0.32	-0.15; 0.15	0.973	Equivalent
	SUVpeak	0.00 ± 0.30	-0.14; 0.14	0.995	Equivalent
	SUVmean	0.04 ± 0.32	-0.15; 0.15	0.995	Equivalent

Table 3 - Difference in SUVs in tumor lesions

		Mean difference mCT-Vision SUV±SD	95% CI	P	Equivalence
Lesions (EARL)	SUVmax	0.09 ± 4.09	-1.24; 1.17	0.956	Equivalent
	SUVpeak	0.07 ± 2.32	-0.69; 0.67	0.985	Equivalent
	SUVmean	0.67 ± 5.41	-1.60; 1.58	0.988	Equivalent
Lesions (clinical)	SUVmax	-6.30 ± 11.75	-3.52; 3.38	0.969	Equivalent
	SUVmax*			<0.001	Not Equivalent
	SUVpeak	0.62 ± 4.04	-1.27; 1.10	0.885	Equivalent
	SUVmean	-2.68 ±6.43	-1.90; 1.90	0.991	Equivalent

* Since the difference between measured SUVmax from the locally preferred clinical reconstructed images between systems was not normally distributed (but skewed), the results of the Wilcoxon signed-rank test were included as well

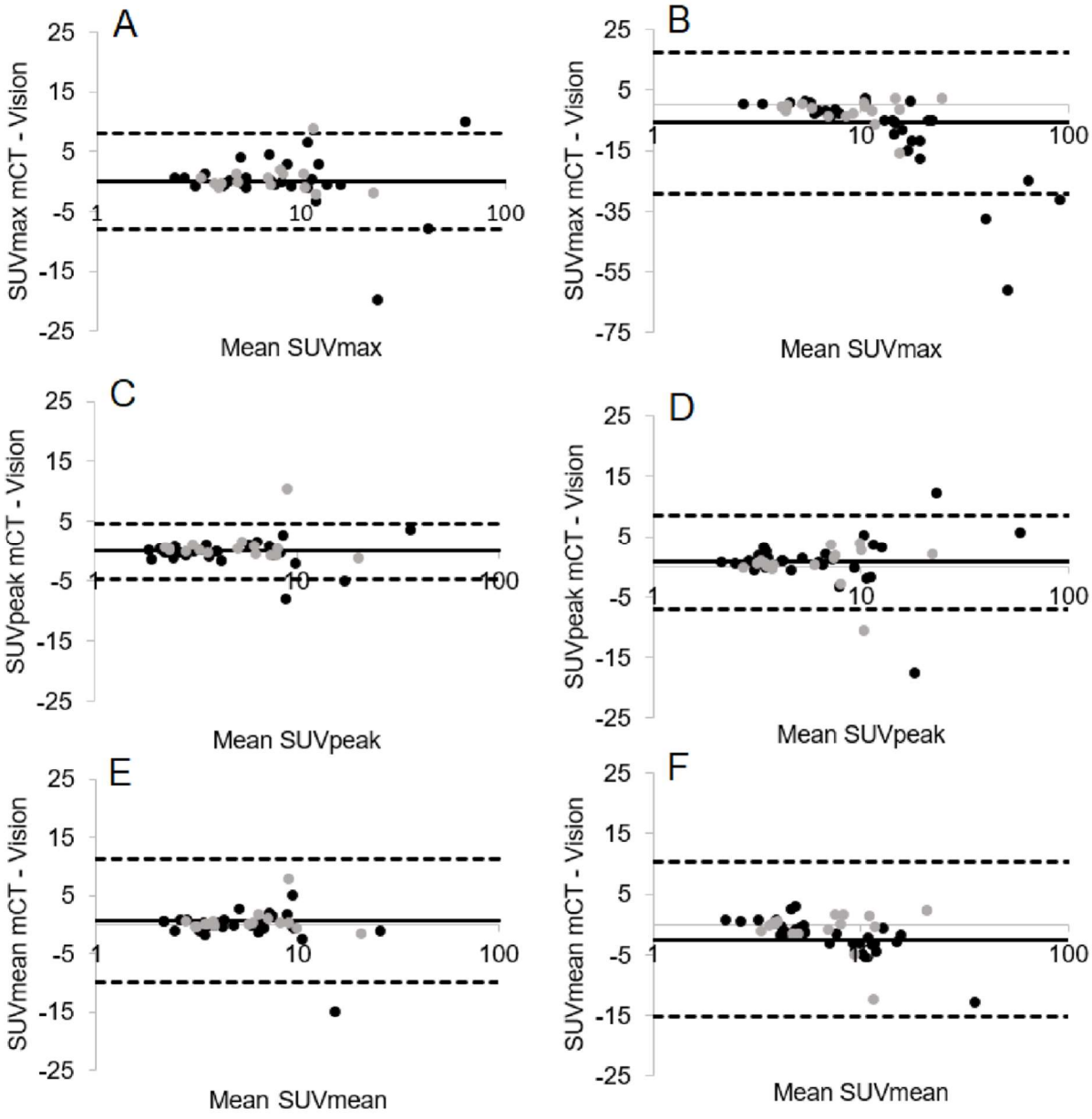

Figure 5 - A Bland-Altman plot of Biograph mCT and Biograph Vision SUVmax lesion measurement differences using the EARL compliant image reconstructions (SUVmax measured on the mCT minus SUVmax measured on the Vision) plotted against the mean SUVmax (the mean SUVmax between systems) (A), a Bland-Altman plot of SUVpeak lesion measurement differences plotted against the mean SUVpeak (C), and a Bland-Altman plot of SUVmean lesion measurement differences plotted against the mean SUVmean (E). The mean difference is illustrated by the horizontal solid black line and the upper and lower limits of agreement are shown by the dashed horizontal lines. The measurements performed on the Biograph mCT first and the Biograph Vision first are illustrated with the black and grey dots, respectively.
For a direct comparison with SUVmax, SUVpeak, and SUVmean measurements obtained from the locally preferred clinical reconstructed images, Bland-Altman plots showing the SUV measurement differences have been added in (B), (D), and (F), respectively.

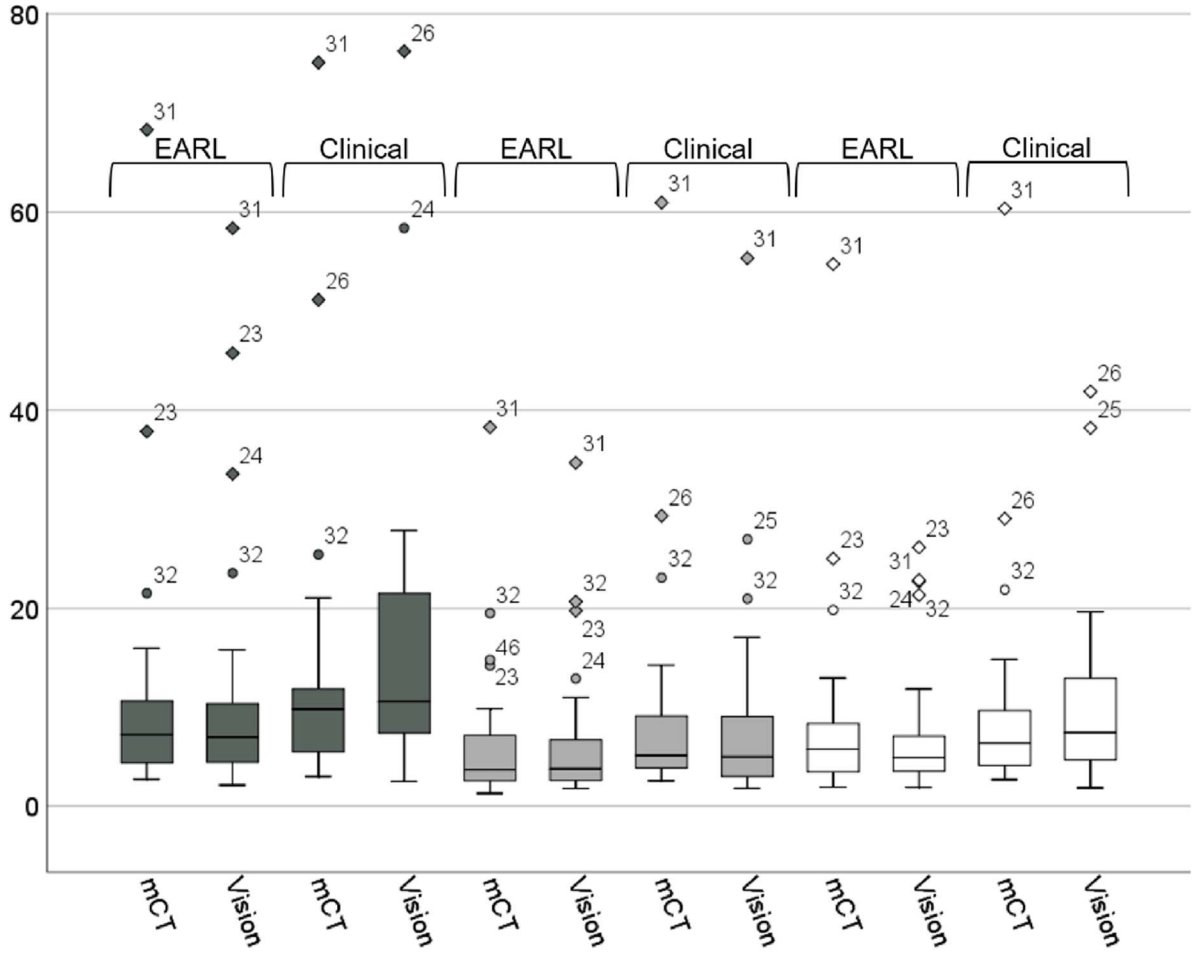

Figure 6 - Boxplots showing the SUVmax (dark grey), SUVpeak (light grey), and SUVmean (white) distributions between EARL compliant (EARL) and locally preferred clinical reconstructed images (clinical) acquired on the Biograph mCT and the Biograph Vision system. Outliers are illustrated with dots, the diamonds represent extreme outliers. For clarity reasons, the vertical scale was set from 0 to 80, consequently, a few outliers are not visible in the boxplots (but can be found in the Bland-Altman plots in Figure 5).